

# Hyperfine structure in the microwave spectra of ultracold polar molecules

Hong Ran

*Department of Chemistry, Durham University, South Road, Durham, DH1 3LE, United Kingdom and  
Institute of Theoretical and Computational Chemistry, Key Laboratory of Mesoscopic Chemistry,  
School of Chemistry and Chemical Engineering, Nanjing University, Nanjing 210093, China*

J. Aldegunde\*<sup>†</sup> and Jeremy M. Hutson<sup>‡</sup>

*Department of Chemistry, Durham University, South Road, Durham, DH1 3LE, United Kingdom*

(Dated: October 31, 2018)

We investigate the microwave spectra of ultracold alkali metal dimers in magnetic, electric and combined fields, taking account of the hyperfine structure due to the nuclear spins. We consider the molecules  $^{41}\text{K}^{87}\text{Rb}$  and  $^7\text{Li}^{133}\text{Cs}$ , which are the targets of current experiments and demonstrate two extremes of large and small nuclear quadrupole coupling. We calculate the frequencies and intensities of transitions that may be used to transfer ultracold molecules between hyperfine states in a magnetic field, employing different polarizations of microwave radiation. In an electric field, the hyperfine levels display narrow avoided crossings at specific fields that we explain in terms of molecular alignment. The hyperfine splittings that arise in electric fields may hinder individual addressing in schemes to use ultracold molecules in quantum computation, but the structure of the spectra is suppressed in combined fields.

PACS numbers: 33.15.Pw, 31.15.aj, 37.10.Pq, 03.67.Lx

## I. INTRODUCTION

Ultracold molecules have potential applications in many areas of physics, ranging from precision measurement to quantum computing [1]. It has recently become possible to create ultracold alkali metal dimers in their ground rovibrational state in ultracold atomic gases, by magnetoassociation followed by state transfer using stimulated Raman adiabatic passage (STIRAP). This has been achieved for both polar  $^{40}\text{K}^{87}\text{Rb}$  [2] and nonpolar  $\text{Cs}_2$  [3] and triplet  $^{87}\text{Rb}_2$  [4], and several other systems are being pursued [5, 6, 7]. It is also now possible to produce low-lying molecular states by direct photoassociation [8, 9, 10, 11, 12].

Alkali metal dimers have a rich spin structure because of the presence of two nuclei with non-zero spin. The nuclear spins interact with one another and with the molecular rotation through several different terms in the hyperfine Hamiltonian. In previous work, we have explored the hyperfine structure, and the effect of applied electric and magnetic fields, for both polar [13] and nonpolar [14] alkali metal dimers.

The microwave spectra of alkali metal dimers are important in a variety of contexts. They provide opportunities to transfer polar molecules between spin states and thus to control the nature of the molecular sample [15]. They are important in proposals to use ultracold

molecules in designs for quantum computers [16, 17, 18], to control intermolecular interactions and create novel quantum phases [19, 20, 21], in condensed-phase models such as the molecular Hubbard Hamiltonian [18, 22], to trap polar molecules using microwave radiation [23] and to use cavity-assisted microwave cooling [24]. However, work on these topics has almost invariably neglected the effects of hyperfine structure.

We have previously given a brief report of the microwave spectrum of  $^{40}\text{K}^{87}\text{Rb}$ , taking account of hyperfine structure and the effects of electric and magnetic fields [25]. The purpose of the present paper is to give a more complete account of the spectra and to extend our predictions to other systems of current experimental interest. In the present paper we compare and contrast the predicted spectra for  $^{41}\text{K}^{87}\text{Rb}$  and  $^7\text{Li}^{133}\text{Cs}$ , which are the targets of current experiments [5, 11] and which demonstrate two extremes of large and small nuclear quadrupole coupling. We concentrate on spectra originating in the rotationless ground state, which is the principal focus of the experimental efforts.

The structure of the paper is as follows. Section II describes the theoretical methods used, while Sections III, IV and V discuss the spectra in the presence of magnetic, electric and combined fields, respectively.

## II. THEORETICAL METHODS

The effective Hamiltonian of a  $^1\Sigma$  molecule in a specified vibrational state consists of rotational, hyperfine, Zeeman and Stark terms [26, 27, 28]. The hyperfine term includes contributions that represent the nuclear electric quadrupole interaction, the nuclear spin-rotation interac-

---

\*Present address: Departamento de Química Física, Facultad de Ciencias Químicas, Universidad de Salamanca, Plaza de los Caídos s/n, 37008, Salamanca, Spain

<sup>†</sup>Electronic address: E-mail: jalde@usal.es

<sup>‡</sup>Electronic address: E-mail: J.M.Hutson@durham.ac.uk

TABLE I: Parameters of the effective Hamiltonians for  $^{41}\text{K}^{87}\text{Rb}$  and  $^7\text{Li}^{133}\text{Cs}$ . Rotational constant ( $B$ ), rotational  $g$ -factor ( $g_r$ ), nuclear  $g$ -factors ( $g_1, g_2$ ) and nuclear quadrupole ( $(eQq)_1, (eQq)_2$ ), shielding ( $\sigma_1, \sigma_2$ ), spin-rotation ( $c_1, c_2$ ), tensor spin-spin ( $c_3$ ) and scalar spin-spin ( $c_4$ ) coupling constants. The subscripts 1 and 2 refer to the more electronegative atom (K or Li) and to the less electronegative one (Rb or Cs) respectively. See ref. 13 for further explanation of the parameters.

	$^{41}\text{K}^{87}\text{Rb}$	$^7\text{Li}^{133}\text{Cs}$
$B$ (GHz)	1.096	5.636
$g_r$	0.0138	0.0106
$g_1$	0.143	2.171
$g_2$	1.834	0.738
$(eQq)_1$ (kHz)	-298	18.5
$(eQq)_2$ (kHz)	-1520	188
$\sigma_1$ (ppm)	1321	108.2
$\sigma_2$ (ppm)	3469	6242.5
$c_1$ (Hz)	10	32
$c_2$ (Hz)	413	3014
$c_3$ (Hz)	21	140
$c_4$ (Hz)	896	1610

tion, and the scalar and tensorial nuclear spin-spin interactions. The Zeeman term is dominated by the nuclear contribution describing the interaction of the nuclei with the magnetic fields. In the present work we construct the Hamiltonian as described in ref. 13 and diagonalize it to obtain the energy levels and wavefunctions.

The hyperfine coupling constants for  $^{41}\text{K}^{87}\text{Rb}$  and  $^7\text{Li}^{133}\text{Cs}$  have been evaluated as described by Aldegunde *et al.* [13]. The resulting values are given in Table I. The calculations were carried out at the equilibrium geometries,  $R_e = 4.07 \text{ \AA}$  for KRb [29] and  $R_e = 3.67 \text{ \AA}$  for LiCs [30]. They are thus most suitable for the vibrational ground state but would also be a reasonable approximation for other deeply bound vibrational states.

There are three sources of angular momentum in a  $^1\Sigma$  molecule: the rotational angular momentum ( $N$ ) and the nuclear spins ( $I_1$  and  $I_2$ ). In the absence of a field, these couple together to give a total angular momentum  $F$ . However, in the presence of electric or magnetic fields,  $F$  is destroyed and the only conserved quantity is the total projection quantum number  $M_F$ . It is most convenient to construct the Hamiltonian in an uncoupled basis set  $|NM_N\rangle|I_1M_1\rangle|I_2M_2\rangle$ , where  $M_N, M_1$  and  $M_2$  are the projections of  $N, I_1$  and  $I_2$  onto the  $z$ -axis defined by the direction of the field.

We consider two different polarizations of the microwave field. When the polarization is parallel to the  $z$ -axis, the selection rules for dipole matrix elements between the uncoupled basis functions are  $\Delta N = \pm 1$ ,  $\Delta M_N = 0$ ,  $\Delta M_1 = 0$ ,  $\Delta M_2 = 0$  and  $\Delta M_F = 0$ . For any other axis of polarization there are components that are circu-

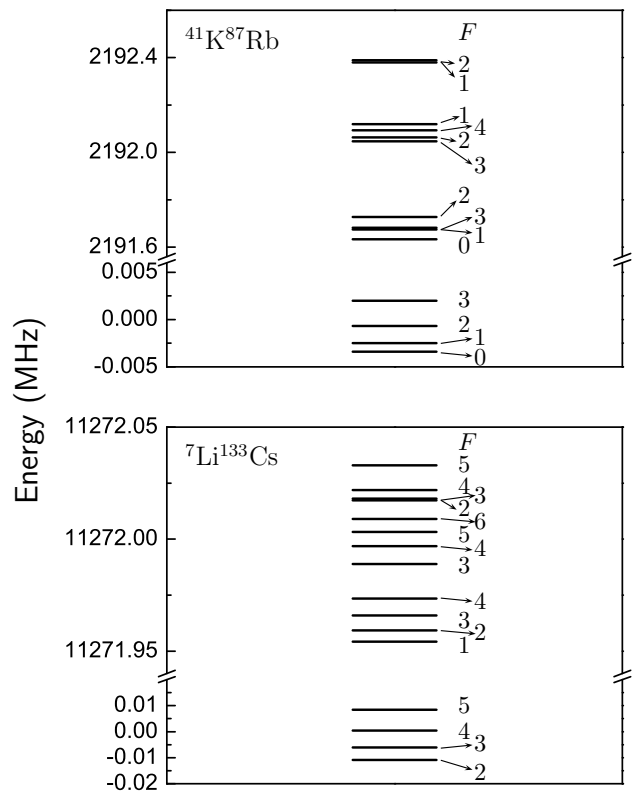


FIG. 1: Zero-field hyperfine splitting for  $^{41}\text{K}^{87}\text{Rb}$  (top panel) and  $^7\text{Li}^{133}\text{Cs}$  (bottom panel). In each panel, the levels below the break correspond to  $N=0$  and the levels above the break to  $N=1$ . The states are labelled by the total angular momentum quantum number  $F$ .

larly polarized with respect to  $z$ ; the selection rules for these components are the same except for  $\Delta M_N = \pm 1$  and  $\Delta M_F = \pm 1$ .

### III. MICROWAVE SPECTRUM IN A MAGNETIC FIELD

The experiments that produce ultracold  $^{40}\text{K}^{87}\text{Rb}$  [2] and  $^{133}\text{Cs}_2$  [3] in their ground rovibrational state involve two main steps. Pairs of ultracold atoms are first associated by sweeping the magnetic field across a zero-energy Feshbach resonance [31, 32]. The resulting Feshbach molecules are then transferred to the ground rovibrational state by stimulated Raman adiabatic passage (STIRAP). The molecules remain in a magnetic field. It is possible in principle to populate a variety of hyperfine levels. However, the current experiments produce dimers with a particular value of  $M_F$  determined by the atomic states used for magnetoassociation, as described below.

An important goal is to control the hyperfine state in which molecules are produced. In particular, the absolute ground state is stable to inelastic collisions with other ground-state species. This section explores how microwave transitions can be used to transfer molecules

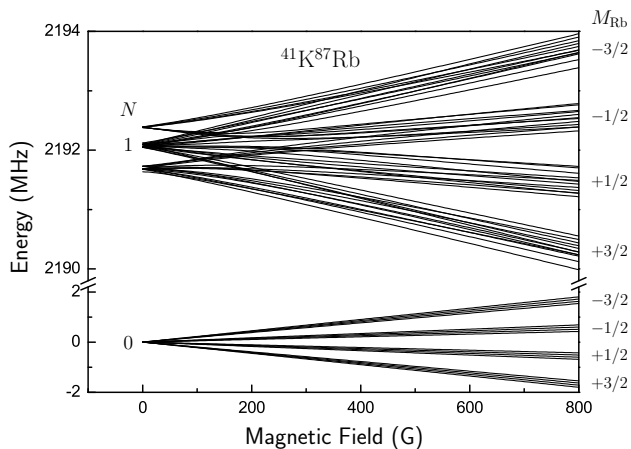


FIG. 2: Zeeman splitting of the  $^{41}\text{K}^{87}\text{Rb}$  hyperfine levels for  $N=0$  and  $N=1$ .

between hyperfine states, as has now been achieved experimentally for  $^{40}\text{K}^{87}\text{Rb}$  [15]. We consider the use of (i)  $z$ -polarized microwave radiation to transfer population between  $N = 0$  states of the same  $M_F$  and (ii) radiation with a circularly polarized component to transfer population into the ground hyperfine state by changing  $M_F$ . We discuss the mechanism of the transfer and the experimental conditions that favor or hinder it.

The zero-field energy level patterns for the  $N=0$  and  $N=1$  levels of  $^{41}\text{K}^{87}\text{Rb}$  and  $^7\text{Li}^{133}\text{Cs}$  are shown in Fig. 1. The levels are labeled by the total angular momentum  $F$ , obtained by coupling the rotational angular momentum  $N$  and the nuclear spins  $I_1$  and  $I_2$ . The nuclear spin is  $3/2$  for  $^{41}\text{K}$ ,  $^{87}\text{Rb}$  and  $^7\text{Li}$  and  $7/2$  for  $^{133}\text{Cs}$ . The splitting of the  $N=0$  states is due to the scalar spin-spin interaction and amounts to just a few kHz. The splitting of the  $N=1$  levels is caused mainly by the nuclear quadrupole interaction and amounts to 800 kHz for  $^{41}\text{K}^{87}\text{Rb}$  and 100 kHz for  $^7\text{Li}^{133}\text{Cs}$ . The difference stems from the very small nuclear quadrupole coupling constants for the  $^7\text{Li}^{133}\text{Cs}$  molecule, attributable to the particularly small values of the electric quadrupoles for the  $^7\text{Li}$  and  $^{133}\text{Cs}$  nuclei [33].

Each of the zero-field levels in Fig. 1 is  $(2F+1)$ -fold degenerate. This degeneracy can be lifted by applying a magnetic field. The energy pattern can be quite complicated as it consists of  $(2N+1)(2I_1+1)(2I_2+1)$  states for each rotational level  $N$ . Fig. 2 shows the Zeeman splitting for the  $N=0$  and 1 hyperfine levels of  $^{41}\text{K}^{87}\text{Rb}$  and includes all the 16  $N=0$  and the 48  $N=1$  hyperfine states. For  $^7\text{Li}^{133}\text{Cs}$  the number of levels is even larger and they will not be shown.

We will first analyze transitions driven by a microwave field polarized parallel to the  $z$ -axis, which conserve the projection of the total angular momentum  $M_F$ . Fig. 3 shows the Zeeman splitting and avoided crossings of the  $^{41}\text{K}^{87}\text{Rb}$  ( $M_F=+2$ ) and  $^7\text{Li}^{133}\text{Cs}$  ( $M_F=+4$ ) hyperfine levels. The reason we choose these  $M_F$  values is that magnetoassociation conserves  $M_F$  and is usually carried

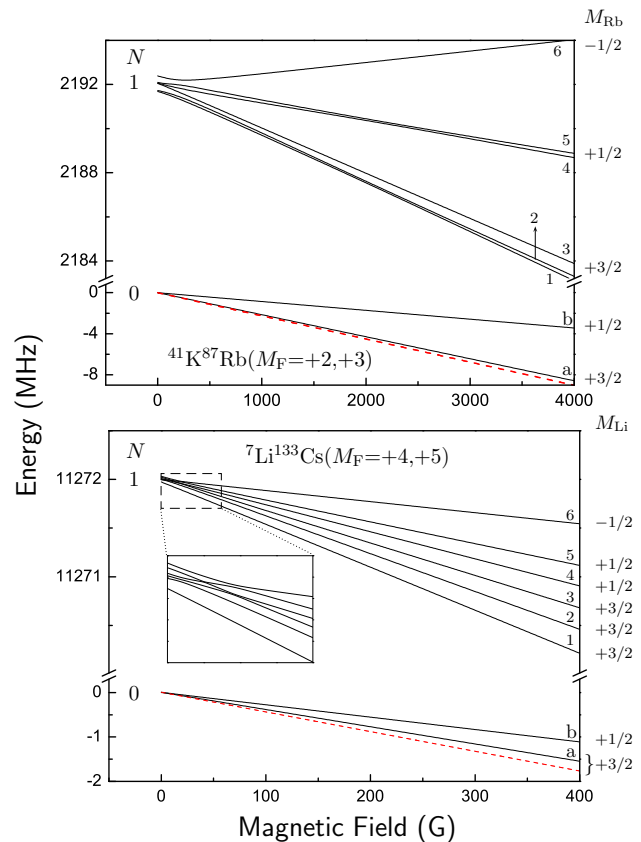


FIG. 3: Zeeman splitting of the hyperfine levels for  $^{41}\text{K}^{87}\text{Rb}$  ( $M_F=+2$ ) and  $^7\text{Li}^{133}\text{Cs}$  ( $M_F=+4$ ). Labels a-b and 1-6 identify the  $N=0$  and  $N=1$  states respectively. The small panel shows an expanded view of the region of avoided crossings for the  $N=1$  levels of  $^7\text{Li}^{133}\text{Cs}$ . The  $^{41}\text{K}^{87}\text{Rb}$  ( $N=0$ ,  $M_F=+3$ ) and  $^7\text{Li}^{133}\text{Cs}$  ( $N=0$ ,  $M_F=+5$ ) levels, which are the absolute ground states except at low magnetic fields, are also included (red dashed lines).

out using atoms in their absolute ground state in the magnetic field, which is  $(f=I-1/2, m_f=I-1/2)$  for all alkali metal atoms except  $^{40}\text{K}$ . This is  $(f=1, m_f=+1)$  for  $^7\text{Li}$ ,  $^{41}\text{K}$ ,  $^{87}\text{Rb}$  and  $(f=3, m_f=+3)$  for  $^{133}\text{Cs}$ . Feshbach molecules are thus likely to be formed initially in  $M_F=+2$  and  $+4$  for  $^{41}\text{K}^{87}\text{Rb}$  and  $^7\text{Li}^{133}\text{Cs}$  respectively. In current experimental configurations, the STIRAP process used to transfer the molecules to the rovibrational ground state also conserve  $M_F$ . The hyperfine state formed in this way is not generally the absolute ground state, which has  $M_F=I_1+I_2$ .

There are important differences between dimers that contain  $^{40}\text{K}$  and those that do not.  $^{40}\text{K}$  is the only stable isotope of any alkali metal to have a negative  $g$ -factor and an inverted hyperfine structure. Because of this, the atomic ground state in a magnetic field is  $(f=I_K+1/2=9/2, m_f=-9/2)$  and heteronuclear Feshbach molecules formed from ground-state atoms have  $M_F=I_1-5$  [34]. The lowest molecular hyperfine state at high magnetic field has  $M_F=I_1-I_K$  because of the nega-

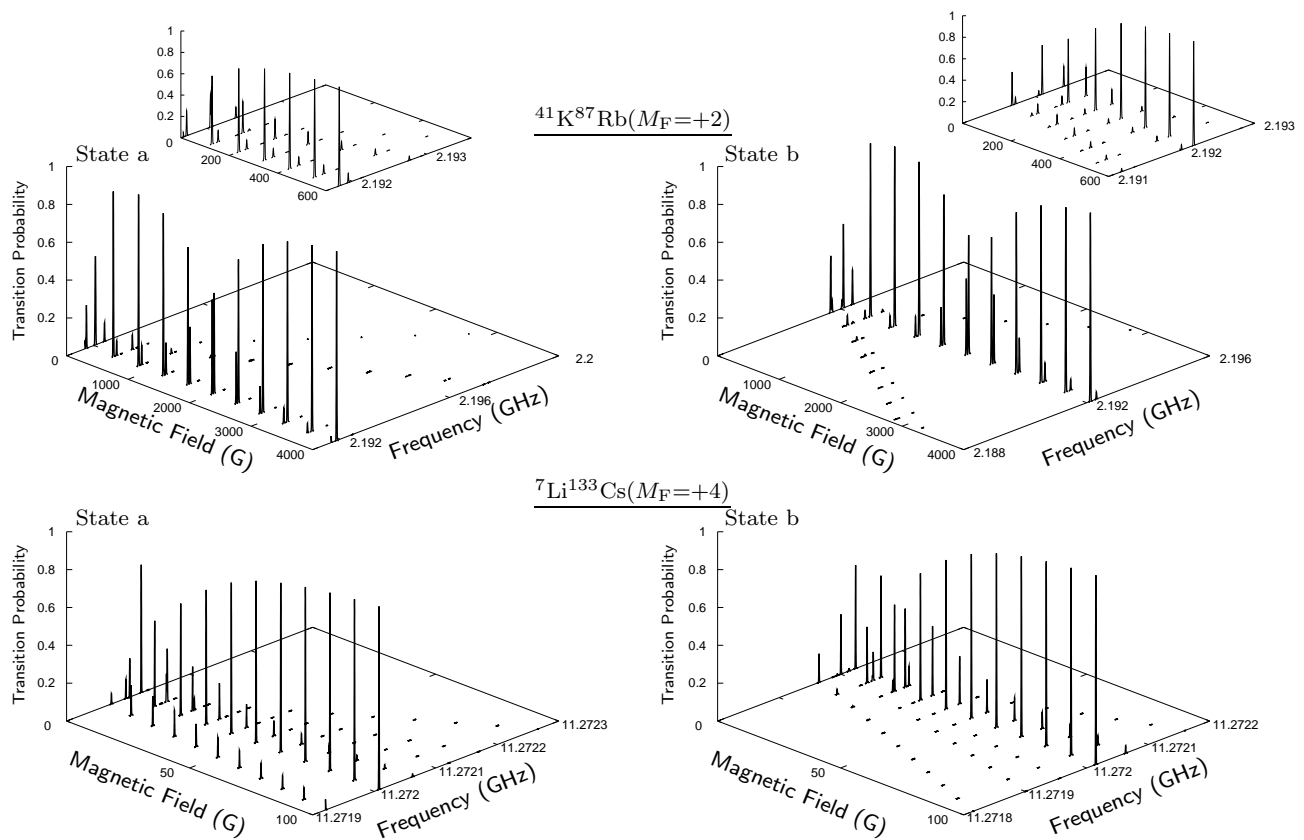


FIG. 4: Relative intensity for the microwave transitions from the two  $N=0$  hyperfine states (levels a and b) to the  $N=1$  hyperfine states (levels 1-6) for  $^{41}\text{K}^{87}\text{Rb}$  ( $M_F=+2$ ) (top panels) and  $^7\text{Li}^{133}\text{Cs}$  ( $M_F=+4$ ) (bottom panels). Enlargements of the 0-600 G region for  $^{41}\text{K}^{87}\text{Rb}$  are shown. The microwave radiation is polarized parallel to the magnetic field. The most intense transition for each molecule is assigned a peak intensity of 1.

tive value of  $g_K$  for  $^{40}\text{K}$ .

As the magnetic field increases from zero, the levels of each  $F$  split into components labeled by  $M_F$ , as shown in Figs. 2 and 3. Avoided crossings occur between states with the same value of  $M_F$ . While for the  $N=0$  levels the crossings occur at small magnetic fields proportional to  $|c_4/(g_1 - g_2)|$ , for the  $N=1$  states they take place at larger fields because of the larger zero-field splittings. Above the crossings,  $F$  is completely destroyed. For both molecules the  $N=0$  avoided crossings occur at fields below 20 G and are hard to see in Figs. 2 and 3. The  $N=1$  crossings take place at fields that depend on zero-field splittings  $E_0$  divided by factors involving the two nuclear  $g$ -factors. Because of the very small zero-field splittings between some pairs of states, some of the avoided crossings can occur at fields as low as a few Gauss, though others are at much higher fields.

The nuclear Zeeman term, which dominates the Hamiltonian at high field, is diagonal in the uncoupled basis set. Because of this, the individual projections of the nuclear spins  $M_1$  and  $M_2$  become nearly good quantum numbers at sufficiently high field. When the  $g$ -factors for the two nuclei are substantially different, as for  $^{41}\text{K}^{87}\text{Rb}$ , the energy levels for each rotational state separate into

distinct groups as the field increases (see Fig. 2). The  $g$ -factor for  $^{87}\text{Rb}$  is much larger than that for  $^{41}\text{K}$ , so that  $M_{\text{Rb}}$  becomes a nearly good quantum number at much smaller fields than  $M_{\text{K}}$  and the states gather together in groups characterized by a well defined value of  $M_{\text{Rb}}$ : the lowest set corresponds to  $M_{\text{Rb}}=+3/2$  and the top set to  $M_{\text{Rb}}=-3/2$ . Similar behavior was observed for  $^{40}\text{K}^{87}\text{Rb}$  in ref. 25.

For  $^{41}\text{K}^{87}\text{Rb}$  with  $M_F=+2$  the levels within each group display shallow avoided crossings and  $M_K$  does not become well defined until fields above about 3000 G. For  $^7\text{Li}^{133}\text{Cs}$ , by contrast, the avoided crossings are complete by 40 G. In general, the number of levels in each group is  $N+I_-+1-|M_F-M_+|$ , where  $I_{\pm}$  and  $M_{\pm}$  are quantum numbers for the nucleus with the larger/smaller  $g$ -factor. When there is more than 1 level in a group there may be high-field crossings between them at a field of approximately  $E_0/g_- \mu_N$ , where  $g_-$  is the smaller of the two  $g$ -factors and  $\mu_N$  is the nuclear magneton. For  $^{41}\text{K}^{87}\text{Rb}$  ( $N=1$ ), setting  $E_0$  to the full range of zero-field energies gives an upper bound of about 5500 G, though the highest crossings in Fig. 3 actually occur around 2000 G. For  $^7\text{Li}^{133}\text{Cs}$  the corresponding upper bound is about 140 G.

We now consider the microwave transitions that are

available to transfer molecules between hyperfine states with the same value of  $M_F$ . Fig. 4 shows the spectra for transitions between the two  $N=0$  hyperfine states (levels a and b) and their  $N=1$  counterparts (levels 1-6) for  $^{41}\text{K}^{87}\text{Rb}$  ( $M_F=+2$ ) and  $^7\text{Li}^{133}\text{Cs}$  ( $M_F=+4$ ) as a function of the magnetic field. The microwave field is  $z$ -polarized. Both molecules show a multi-line spectrum at low field but the spectra become dominated by a single transition in the strong-field limit. However, while a 100 G field is enough to cause this change for  $^7\text{Li}^{133}\text{Cs}$ , more than 4000 G is necessary for  $^{41}\text{K}^{87}\text{Rb}$ .

The progression from multi-line spectra to single-line-dominated spectra arises because the selection rules for  $z$ -polarized light only permit transitions

$$|N = 0, M_N, M_1, M_2\rangle \leftrightarrow |N = 1, M_N, M_1, M_2\rangle \quad (1)$$

where the angular momentum projections do not change. At low magnetic fields the  $|N, M_N, M_1, M_2\rangle$  functions are “spread” over different eigenstates and multiple transitions from each  $N=0$  state appear. As the magnetic field increases the eigenstates are better approximated by the  $|N, M_N, M_1, M_2\rangle$  basis functions. This takes place at much lower magnetic fields for  $N=0$  than for  $N=1$ . In the strong-field limit the only permitted transition from each  $N=0$  hyperfine state is given by the selection rule (1). This occurs at lower field for  $^7\text{Li}^{133}\text{Cs}$  than for  $^{41}\text{K}^{87}\text{Rb}$  because  $M_K$  is not a good quantum number until very high field in the latter case.

These spectra are important because they clarify under what conditions the  $N=0 \leftrightarrow N=1$  microwave transitions can be used to transfer population between different  $N=0$  hyperfine states corresponding to the same  $M_F$  through a two-photon process that uses the  $N=1$  levels as intermediate states. This will be feasible if there is at least one  $N=1$  level that displays a significant intensity from both the  $N=0$  states involved in the transfer. This requires substantially smaller magnetic fields for  $^7\text{Li}^{133}\text{Cs}$  than for  $^{41}\text{K}^{87}\text{Rb}$ .

Microwave radiation whose polarization is not parallel to the external field can be used to transfer population between hyperfine states with different  $M_F$ . For  $^{41}\text{K}^{87}\text{Rb}$  and  $^7\text{Li}^{133}\text{Cs}$  the absolute ground state corresponds to  $M_F=+3$  and  $+5$  respectively except at very low magnetic field (see Fig. 3). It is therefore possible to reach the absolute ground state from  $^{41}\text{K}^{87}\text{Rb}$  ( $M_F=+2$ ) and  $^7\text{Li}^{133}\text{Cs}$  ( $M_F=+4$ ) if one of the two photons is circularly polarized. Whether this photon is responsible for the first or the second transition gives rise to two possible experimental implementations.

Fig. 5 shows the spectra for  $M_F$ -changing transitions between the absolute ground states of  $^{41}\text{K}^{87}\text{Rb}$  and  $^7\text{Li}^{133}\text{Cs}$  and the  $N=1$  levels shown in Figs. 3 and 4. In both cases the microwave field is circularly polarized. As for  $\Delta M_F=0$  transitions, there are several lines with significant intensity at low field but a single line dominates at sufficiently high field. The changeover occurs at considerably higher fields for  $^{41}\text{K}^{87}\text{Rb}$  than for  $^7\text{Li}^{133}\text{Cs}$ .

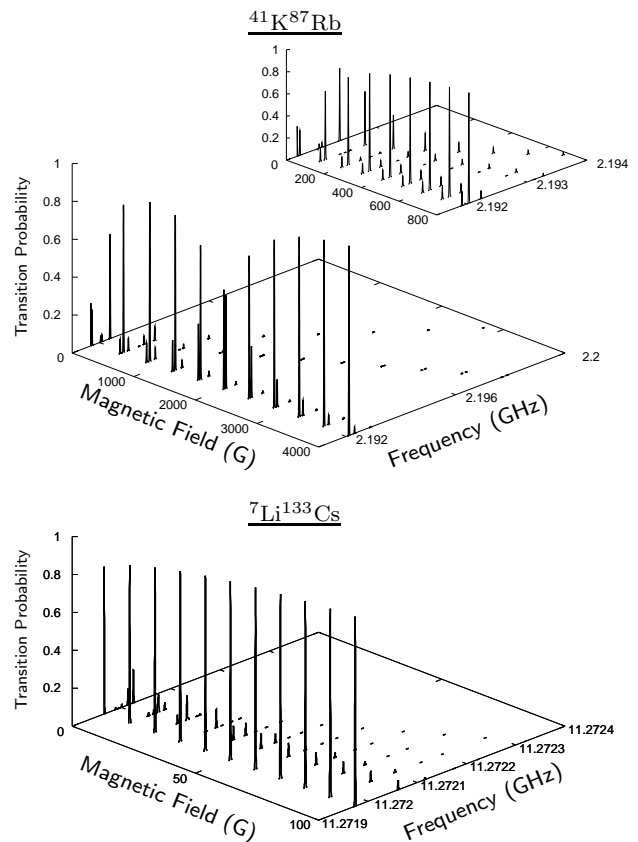


FIG. 5: Relative intensities for the transitions between the ( $N=0, M_F=+3$ ) and ( $N=1, M_F=+2$ ) states of  $^{41}\text{K}^{87}\text{Rb}$  (top panels) and between the ( $N=0, M_F=+5$ ) and ( $N=1, M_F=4$ ) states of  $^7\text{Li}^{133}\text{Cs}$  (bottom panel). The microwave radiation is circularly polarized. The most intense transition for each molecule is assigned a peak intensity of 1.

The propensity rules for the possible paths are summarized in Fig. 6 for  $^7\text{Li}^{133}\text{Cs}$ . Solid, dashed and dotted lines represent transitions where none, one or two nuclear spins projections change and correlate with strong, medium and weak lines in the spectra. For either initial state (a or b), there are several paths to the lowest hyperfine state that combine one strong transition (solid line) with one weaker transition (dashed line). However, it should be noted that the propensity rules become stronger (more like selection rules) as the magnetic field increases. The overall two-photon transfer will therefore be more difficult at high fields and forbidden in the strong-field limit.

The propensity rules are very similar for  $^{41}\text{K}^{87}\text{Rb}$  ( $N=0, M_F=+2 \leftrightarrow N=0, M_F=+3$ ). The number and ordering of the levels and the distribution of strong, medium and weak transitions are identical to those for  $^7\text{Li}^{133}\text{Cs}$ . However, in  $^{41}\text{K}^{87}\text{Rb}$ ,  $M_K$  is not a nearly good quantum number until very high field so the propensity rules are not as strong.

In summary, the transfer of population between different  $N=0$  hyperfine states using microwave transi-

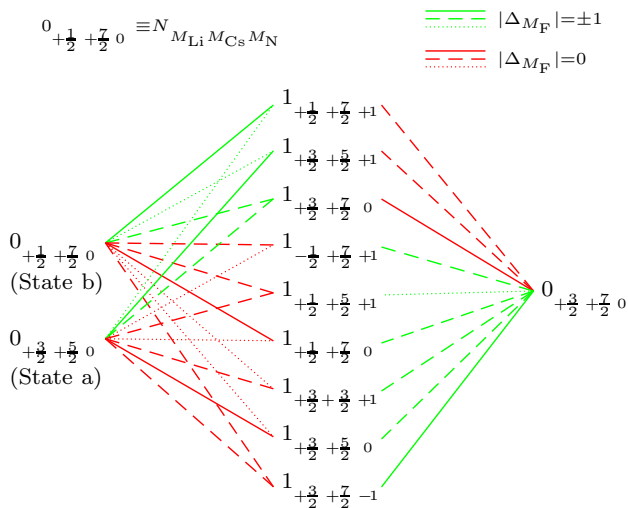


FIG. 6: Propensity rules for the transitions available to transfer  ${}^7\text{Li}{}^{133}\text{Cs}$  between the ( $N=0$ ,  $M_F=+4$ ) states (a and b, left side) and the absolute ground state with  $M_F=+5$  (right side) via  $N=1$  levels with  $M_F=+4$  and  $+5$  (center). In the left column the energy levels are ordered according to their energy in the strong-field region and in the central column the 6 (3)  $M_F=+4$  (5)  $N=1$  levels are shown separately at the bottom (top) and then ordered by the same criterion. Green (red) lines indicate transitions driven by circularly ( $z$ ) polarized light. Solid, dashed and dotted lines represent transitions where none, one or two nuclear spin projections change and correspond to strong, medium and weak lines in the spectra.

tions will be facilitated by a larger mixture between the  $|N=1, M_N, M_1, M_2\rangle$  basis functions, which can be achieved by carrying out the transfer at low magnetic fields. The actual fields required depend on the magnitudes of the nuclear quadrupole coupling constants and the nuclear  $g$ -factors. The transfer is not possible in the limiting strong-field region.

#### IV. MICROWAVE SPECTRUM IN AN ELECTRIC FIELD

The microwave spectra of ultracold molecules in electric fields are important in many contexts, ranging from quantum information processing [16, 17, 18] to the creation of novel quantum phases [19, 20]. In this section we explore the effect of hyperfine structure on these spectra, focusing particularly on the relevance for implementation of a quantum computer.

The features of the spectrum in the presence of an electric field will differ drastically from those found for a magnetic field. Electric fields do not conserve parity and cause strong mixing of rotational levels. The strength of the Stark effect depends on the molecular electric dipole moment  $\mu$ , 0.57 D for KRb [2] and 5.5 D for LiCs [35].

DeMille has proposed a quantum computing implementation in which the qubits are ultracold alkali dimers oriented along  $(|0\rangle)$  or against  $(|1\rangle)$  an external electric

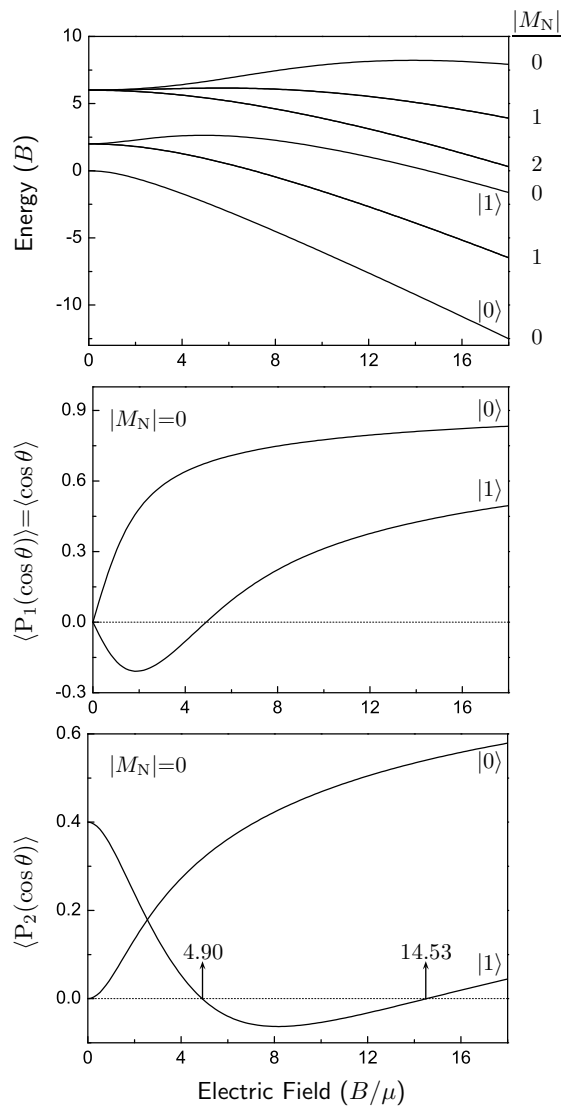


FIG. 7: Stark energy levels for a  ${}^1\Sigma$  diatomic molecule correlating with  $N=0$  to 2 (top panel). The labels  $|0\rangle$  and  $|1\rangle$  identify the levels used as qubits. The hyperfine structure is not included. The central and bottom panels show the expectation values of the Legendre polynomials  $P_1(\cos \theta)$  and  $P_2(\cos \theta)$  for  $|0\rangle$  and  $|1\rangle$ .

field [16]. The field strength changes with the position in the device so as to allow individual addressing of the molecules, which is performed using microwave transitions. The  $|0\rangle$  and  $|1\rangle$  states are mixtures of the  $M_N=0$  levels that correlate with  $N=0$  and 1 respectively at zero field. The goal of this section is to ascertain whether the hyperfine structure will interfere with the addressing process.

The top panel of Fig. 7 shows the lowest Stark energy levels of a  ${}^1\Sigma$  diatomic molecule, neglecting nuclear spin, as a function of the reduced field in units of  $B/\mu$ , where  $B$  is the rotational constant of the molecule. The electric field orients the molecule and produces a space-fixed dipole moment  $d = \mu \langle \cos \theta \rangle$ , where  $\theta$  is the angle be-

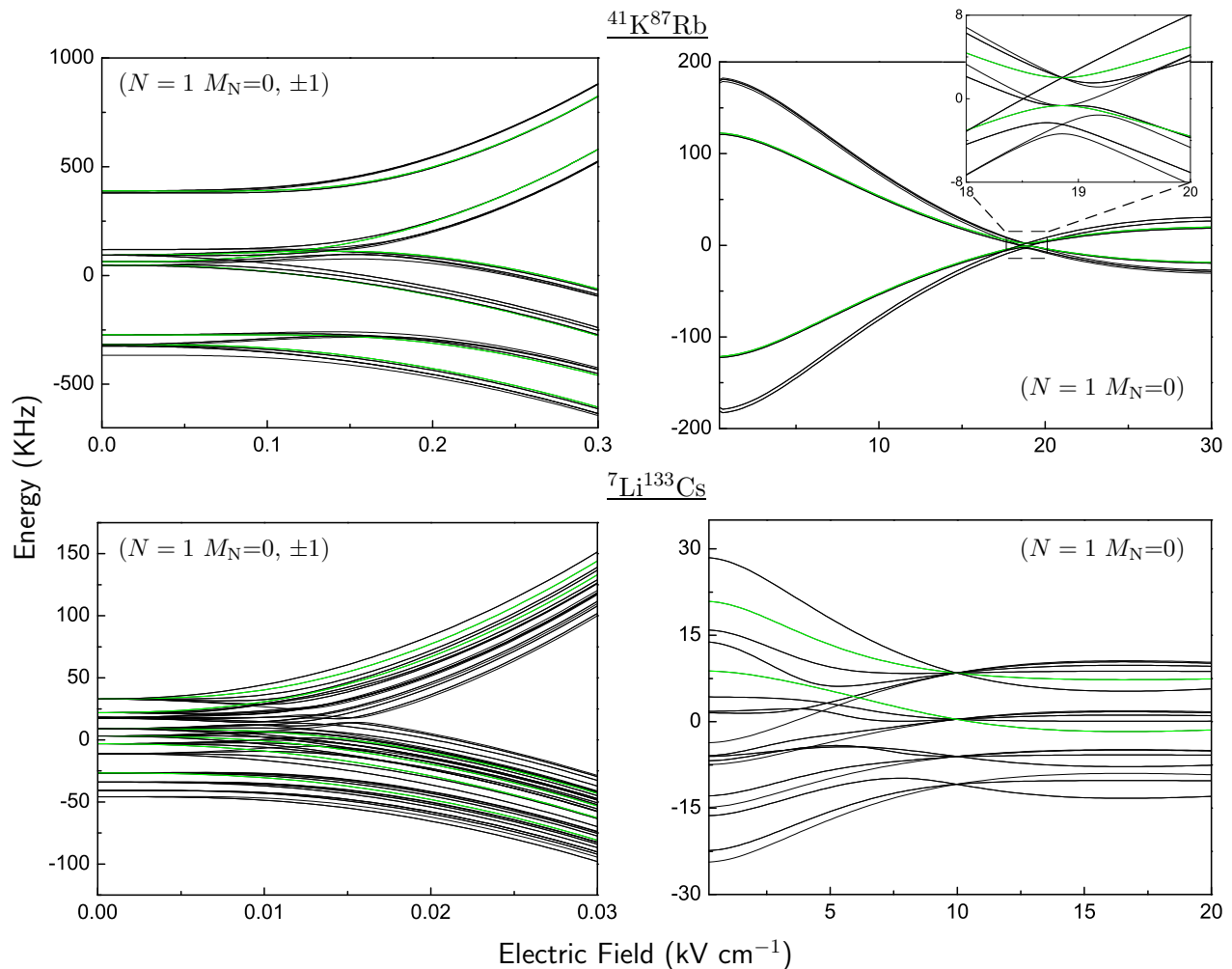


FIG. 8: Stark splitting of the hyperfine levels correlating with  $N=1$  for  $^{41}\text{K}^{87}\text{Rb}$  (upper panels) and  $^7\text{Li}^{133}\text{Cs}$  (lower panels). The left-hand panels include all the hyperfine states and show the low-field region where the electric field separates the  $|M_N|=0$  (upper branch) and 1 (lower branch) levels. The right-hand panels show the splitting for the  $M_N=0$  states. The levels in each panel are shown relative to their field-dependent average energy and those corresponding to  $^{41}\text{K}^{87}\text{Rb}$  ( $M_F=+2$ ) and  $^7\text{Li}^{133}\text{Cs}$  ( $M_F=+4$ ) are shown in green.

tween the internuclear axis and the electric field. The central panel in Fig. 7 shows the degree of *orientation*, defined as the expectation value of  $\cos\theta$ , for the states  $|0\rangle$  and  $|1\rangle$ . For electric fields in the interval  $(2-5)B/\mu$ , the operating range of fields in DeMille's proposal, the  $|0\rangle$  ( $|1\rangle$ ) state corresponds to an orientation of the permanent dipole parallel (antiparallel) to the direction of the field. In the strong-field limit, the expectation value approaches unity for both molecular states, corresponding to a perfectly parallel orientation of the dipole.

As in Section III, we begin by analyzing the behavior of the energy levels. Because of the choice for  $|0\rangle$  and  $|1\rangle$ , we focus on  $M_N=0$  states and transitions driven by a  $z$ -polarized microwave field.

Fig. 8 shows the Stark splitting of the hyperfine levels correlating with  $N=1$  for  $^{41}\text{K}^{87}\text{Rb}$  and  $^7\text{Li}^{133}\text{Cs}$ . The field-dependent average energy has been subtracted so that the hyperfine structure can be appreciated. Small

electric fields, 0.3 kV/cm for  $^{41}\text{K}^{87}\text{Rb}$  and 0.02 kV/cm for  $^7\text{Li}^{133}\text{Cs}$ , are enough to make  $M_N$  a nearly good quantum number and to separate the  $|M_N|=0$  and 1 energy levels.

The  $M_N=0$  states display a striking feature as a function of the electric field. At a field of 18.8 kV/cm for  $^{41}\text{K}^{87}\text{Rb}$  or 9.95 kV/cm for  $^7\text{Li}^{133}\text{Cs}$ , all the levels come very close together and almost cross. At this point the hyperfine splitting reduces to that caused by the (very small) scalar spin-spin interaction, as shown in the inset for  $^{41}\text{K}^{87}\text{Rb}$ . The effects of the nuclear quadrupole, the scalar spin-spin and the nuclear spin-rotation interactions vanish and the splitting simplifies and coincides with that found for the  $N=0$  levels in the absence of fields. At this point the total nuclear spin obtained by coupling  $I_1$  and  $I_2$  is a good quantum number. In addition to their effect on the microwave spectra, such close avoided crossings may cause nonadiabatic transitions for molecules in time-varying electric fields.

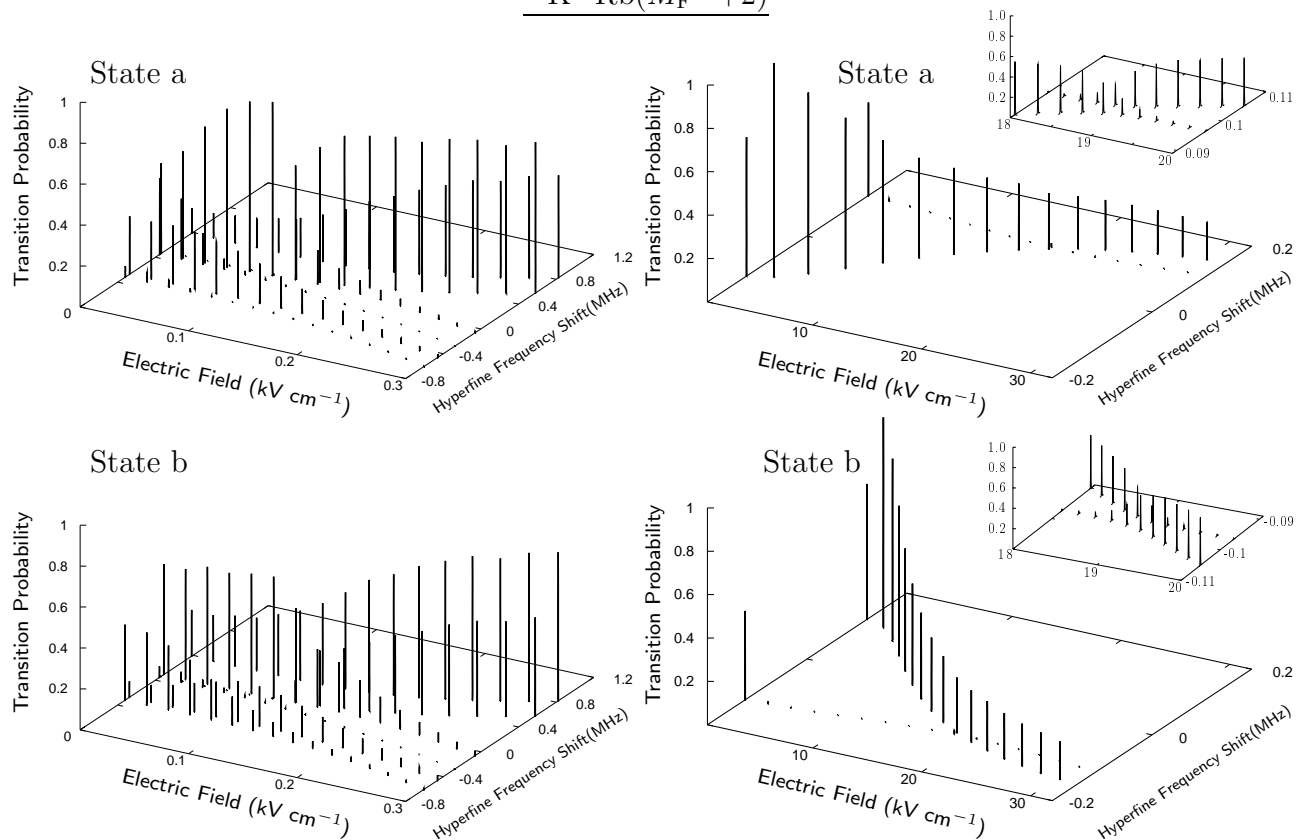
$$^{41}\text{K}^{87}\text{Rb}(M_F=+2)$$


FIG. 9: Relative intensities for the transitions between the levels correlating with  $N=0$  (states a and b) and  $N=1$  for  $^{41}\text{K}^{87}\text{Rb}$  ( $M_F=+2$ ). The microwave field is polarized parallel to the electric field. The left-hand panels show the spectra for low electric fields where  $M_N$  is not yet a good quantum number. The right-hand panels show spectra at higher fields where  $M_N$  is well defined and only transitions to the ( $N=1$ ,  $M_N=0$ ) branch are permitted. In order to keep the spectrum on a single frequency scale as a function of the electric field, we plot the hyperfine frequency shift instead of the absolute frequency. This is obtained by subtracting the frequency for the transition in the absence of hyperfine splittings. The most intense transition is assigned a peak intensity of 1.

Near-crossings like those shown in Fig. 8 will be a universal feature for polar molecules in  $^1\Sigma$  states. The nuclear quadrupole interaction depends on the electric field gradient created by the electrons at the positions of the nuclei. This is a cylindrically symmetric second-rank tensor  $V_q^{(2)}$  with only a  $q=0$  component in the molecule-fixed frame. However, the nuclei experience the electric field gradient in the space-fixed frame, with components  $V_p^{(2)}$  given by

$$V_p^{(2)} = D_{p0}^2(\phi, \theta, 0)V_{q=0}^{(2)}, \quad (2)$$

where  $D_{p0}^2(\phi, \theta, 0)$  is a Wigner rotation matrix and  $\phi$  is the azimuthal angle. For the  $M_N=0$  levels, only the component with  $p=0$  has diagonal matrix elements, and  $D_{00}^2(\phi, \theta, 0) = P_2(\cos\theta)$ , the second Legendre polynomial. The time-averaged field gradient is thus proportional to the degree of *alignment*, defined as  $\langle P_2(\cos\theta) \rangle$ . As shown in the bottom panel of Fig. 7, this passes through zero for state  $|1\rangle$  at two specific values of the electric field. The first zero occurs at an electric field

equal to  $4.90 B/\mu$  and coincides with the points where the hyperfine structure simplifies in Fig. 8. The second zero appears at larger fields ( $14.53 B/\mu$ ) that are outside the range plotted in Fig. 8. The tensorial spin-spin interaction is also proportional to  $\langle P_2(\cos\theta) \rangle$ , so vanishes at the same point, while the nuclear spin-rotation interaction has no diagonal matrix elements for  $M_N=0$  at any value of the field.

For the  $|0\rangle$  state, which correlates with  $N=0$ ,  $\langle P_2(\cos\theta) \rangle$  increases monotonically with field, from zero at zero field to unity in the high-field limit. The nuclear quadrupole and tensorial spin-spin splittings thus also increase monotonically and there are no close avoided crossings [13].

Close avoided crossings such as those shown in Fig. 8 might also cause nonadiabatic transitions between hyperfine states for molecules in time-varying electric fields. This might occur either when sweeping an electric field or for molecules moving in an inhomogeneous field.

Figures 9 and 10 show the hyperfine transitions driven



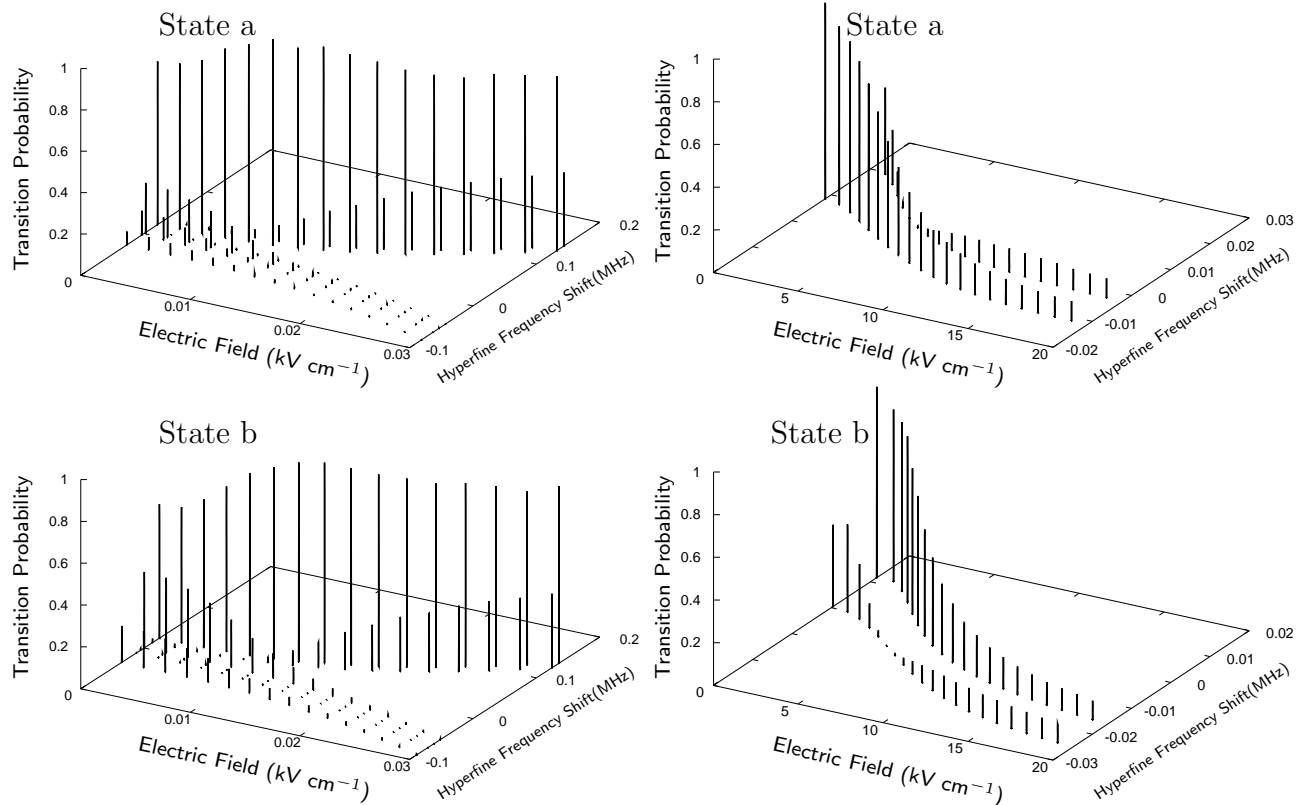
$${}^7\text{Li}^{133}\text{Cs}(M_F=+4)$$


FIG. 10: Relative intensities for the transitions between the levels correlating with  $N=0$  (states a and b) and  $N=1$  for  ${}^7\text{Li}^{133}\text{Cs}$  ( $M_F=+4$ ). The microwave field is polarized parallel to the electric field. The left-hand panels show the spectra for low electric fields where  $M_N$  is not yet a good quantum number. The right-hand panels show spectra at higher fields where  $M_N$  is well defined and only transitions to the ( $N=1, M_N=0$ ) branch are permitted. In order to keep the spectrum on a single frequency scale as a function of the electric field, we plot the hyperfine frequency shift instead of the absolute frequency. The most intense transition is assigned a peak intensity of 1.

by a  $z$ -polarized microwave field ( $\Delta M_F=0$ ) between the  $N=0$  (states a and b) and  $N=1$  hyperfine states of  ${}^{41}\text{K}^{87}\text{Rb}$  ( $M_F=+2$ ) and  ${}^7\text{Li}^{133}\text{Cs}$  ( $M_F=+4$ ) respectively. The left-hand panels in these figures present blow-ups of the weak-field regions of the spectra, where the separation between the  $|M_N|=0$  and 1 levels takes place. At very low fields  $M_N$  is not a good quantum number and the six  $N=1$  hyperfine levels can all be reached from both states a and b. However, as the electric field increases  $|M_N|$  becomes better defined and the transition intensity concentrates in the  $M_N=0$  branch (at higher frequency). This happens at smaller electric fields for  ${}^7\text{Li}^{133}\text{Cs}$  due to its larger electric dipole moment.

The right-hand panels of Figs. 9 and 10 show the hyperfine structure of the spectra at larger fields, where only transitions into the two ( $N=1, M_N=0$ ) levels are permitted. These figures include the range of fields where DeMille's quantum computing scheme would operate: 7.7 to 19.3 kV/cm for  ${}^{41}\text{K}^{87}\text{Rb}$  and 6.1 to 10.2 kV/cm for  ${}^7\text{Li}^{133}\text{Cs}$ .

If the alkali dimers are going to work as qubits, it must

be possible to switch repeatedly between the  $|0\rangle$  and  $|1\rangle$  states without exciting any other state of the molecule and without altering the state of neighboring molecules. The hyperfine structure will complicate the operation by making these conditions more difficult to fulfil: Figs. 9 and 10 show that for both molecules the spectra display several transitions with significant intensity at each field in the working range. The simulation of the spectrum for  ${}^{41}\text{K}^{87}\text{Rb}$  in the region where the ( $N=0, M_N=0$ ) states cross, 18 to 20 kV/cm, displays two lines with approximately the same intensity. The insets of Fig. 9 show a blowup of this region. The hyperfine structure will also hinder the operation of the device at electric fields below the crossings: the intensity of the weaker transition is significant, mostly  $\geq 10^{-4}$  of that of the main peak, and the two lines spread over a range of frequency shifts comparable to the frequency step used for addressing (250 kHz). The spectrum for  ${}^7\text{Li}^{133}\text{Cs}$  (Fig. 10) has different features. It shows two intense lines for the whole range of electric fields. Both peaks are compressed in a 10 kHz interval of frequency shifts, well below the addressing step

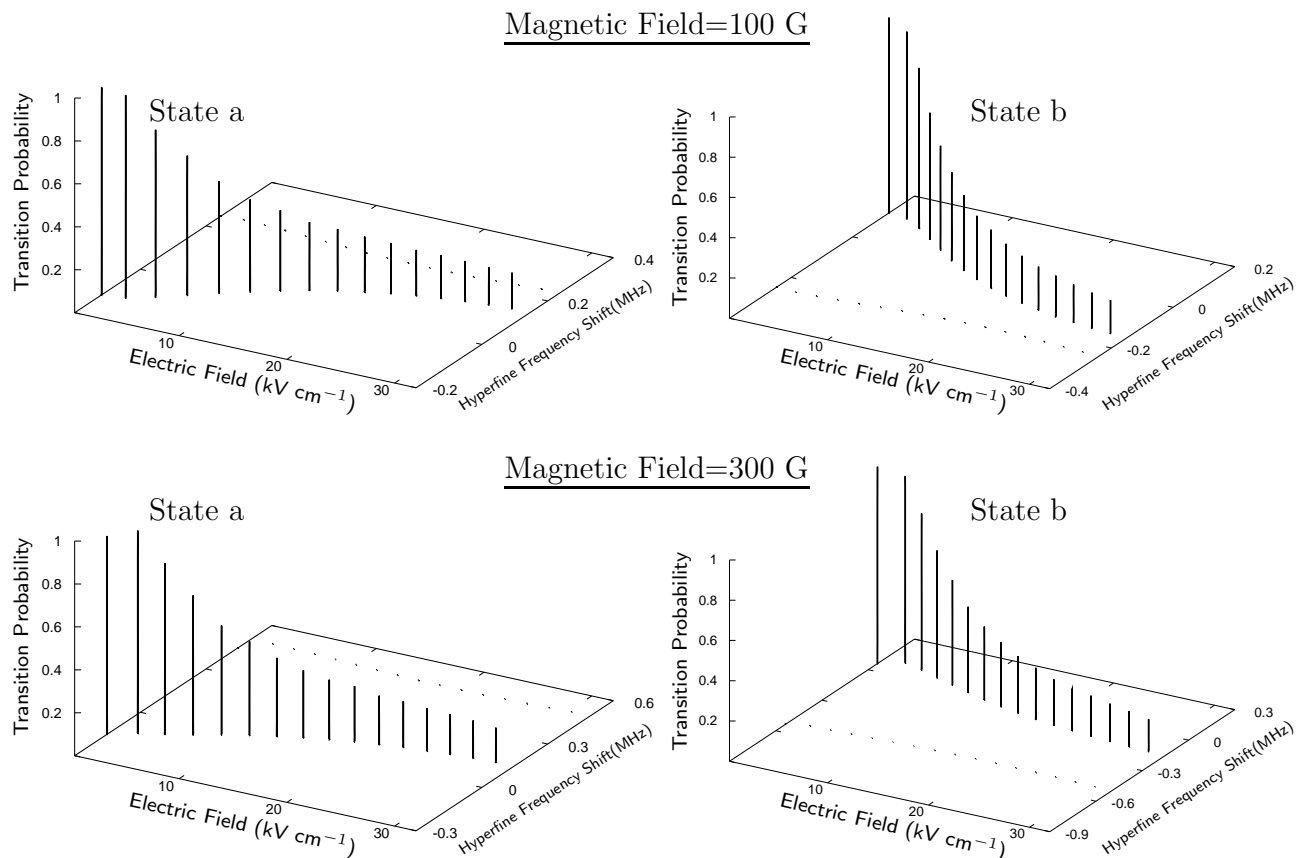


FIG. 11: Relative intensities for the transitions between the  $M_N=0$  levels correlating with  $N=0$  (states a and b) and  $N=1$  for  $^{41}\text{K}^{87}\text{Rb}$  ( $M_F=+2$ ) in parallel electric and magnetic fields. The lowest electric field shown is  $0.3 \text{ kV cm}^{-1}$ . The microwave field is polarized parallel to the external fields. In order to keep the spectrum on a single frequency scale as a function of the electric field, we plot the hyperfine frequency shift instead of the absolute frequency. The most intense transition for each value of the magnetic field is assigned a peak intensity of 1.

for this molecule (1.7 MHz).

The different behavior in the relative intensities for  $^{41}\text{K}^{87}\text{Rb}$  and  $^7\text{Li}^{133}\text{Cs}$  can be rationalized in terms of the following rules (which apply only to  $M_N=0$  states). For molecules where the nuclear quadrupole interaction dominates the other hyperfine terms and one of the nuclear quadrupole coupling constants is much larger than the other, the individual nuclear spin projections  $M_1$  and  $M_2$  are nearly good quantum numbers for any electric field large enough to make the  $|M_N|\neq 0$  contributions negligible. The electric field not only causes the state to be dominated by  $M_N=0$  but also indirectly makes  $M_1$  and  $M_2$  well defined. This explains why for  $^{41}\text{K}^{87}\text{Rb}$  one transition is much more intense than the other except in the low-field and the crossing regions.  $^{40}\text{K}^{87}\text{Rb}$  [25] is similar in this respect. By contrast, if the nuclear quadrupole interaction is not dominant or if the two nuclear quadrupole coupling constants are similar,  $M_1$  and  $M_2$  do not become well defined as the field increases. In this case more than one intense line will appear even at high fields, as in the case of  $^7\text{Li}^{133}\text{Cs}$ .

In summary, the individual addressing of alkali dimers in a quantum computing device such as that proposed

by DeMille [16] may be hindered by the existence of hyperfine structure. For molecules with large nuclear quadrupole constants, the hyperfine spectra of adjacent molecules may overlap, introducing an additional complication to the operation of the device.

## V. MICROWAVE SPECTRUM IN COMBINED ELECTRIC AND MAGNETIC FIELDS

Combining electric and magnetic fields provides an additional degree of control over molecular properties and interactions. In this section we explore the effects of applying parallel electric and magnetic fields on the microwave spectra.

Figures 11 and 12 show the hyperfine transitions between  $N=0$  (states a and b) and  $N=1$  levels of  $^{41}\text{K}^{87}\text{Rb}$  ( $M_F=+2$ ,  $M_N=0$ ) and  $^7\text{Li}^{133}\text{Cs}$  ( $M_F=+4$ ,  $M_N=0$ ) as a function of electric field for different values of the magnetic field. The two molecules show quite similar behavior. A magnetic field resolves the near-degeneracy of the ( $N=1$ ,  $M_N=0$ ) states with different values of  $M_1$  and  $M_2$ . Once  $M_1$  and  $M_2$  become nearly good quantum numbers,

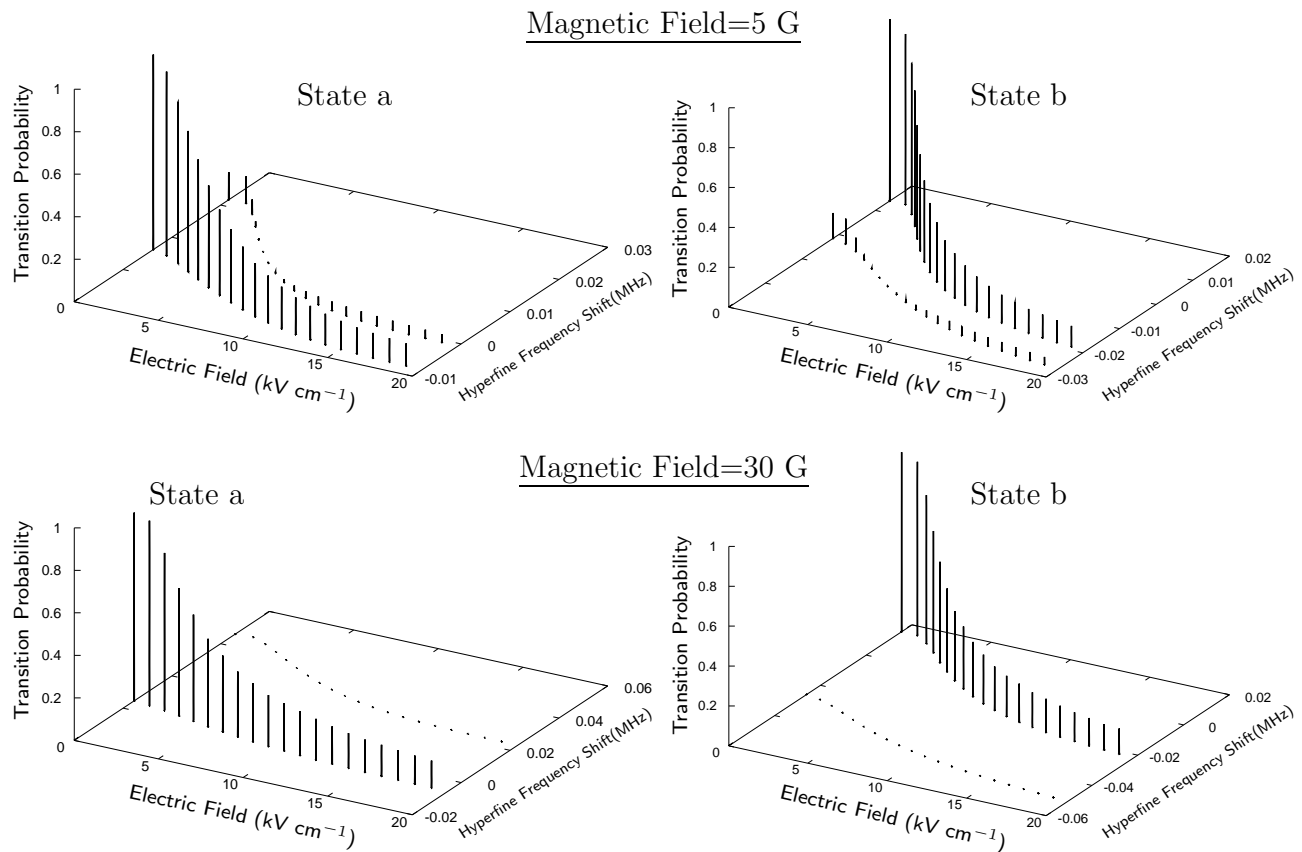


FIG. 12: Relative intensities for the transitions between the  $M_N=0$  levels correlating with  $N=0$  (states a and b) and  $N=1$  for  ${}^7\text{Li}^{133}\text{Cs}$  ( $M_F=+4$ ) in parallel electric and magnetic fields. The lowest electric field shown is  $0.03 \text{ kV cm}^{-1}$ . The microwave field is polarized parallel to the external fields. In order to keep the spectrum on a single frequency scale as a function of the electric field, we plot the hyperfine frequency shift instead of the absolute frequency. The most intense transition for each value of the magnetic field is assigned a peak intensity of 1.

the spectrum is dominated by a single line. Even a relatively small magnetic field is sufficient to achieve this for both molecules, and there are no shallow avoided crossings at high magnetic field such as those that appear for  ${}^{41}\text{K}^{87}\text{Rb}$  in the absence of an electric field, as discussed in Section III.

The subsidiary transitions are 6 or 7 orders of magnitude weaker for  ${}^{41}\text{K}^{87}\text{Rb}$  at 500 G or  ${}^7\text{Li}^{133}\text{Cs}$  at 100 G and their intensities continue to decrease at higher magnetic fields. Similar behavior is expected for all other alkali metal dimers. It is therefore possible to produce a single-line-dominated spectrum, with no crossings as a function of electric field, simply by applying an additional magnetic field. The use of combined electric and magnetic fields thus restores the simplicity needed to apply DeMille's quantum computing scheme.

## VI. CONCLUSIONS

We have explored the hyperfine structure of the microwave spectra of ultracold alkali metal dimers in applied magnetic, electric and combined fields, taking full

account of hyperfine structure. We have compared the spectra for  ${}^{41}\text{K}^{87}\text{Rb}$  and  ${}^7\text{Li}^{133}\text{Cs}$ , which have large and small values, respectively, of the nuclear quadrupole coupling constants. Our results can therefore be extrapolated to understand the microwave spectra of any other alkali dimer.

The alkali dimers have very complicated spin structure arising from the presence of two non-zero nuclear spins. Because of this, there are many possible spectra that might be considered. We have focussed mostly on spectra in which the initial hyperfine state has  $N=0$  and the same value of  $M_F$  as Feshbach molecules produced from atoms in their absolute ground states. However, our programs can readily be applied to other  $M_F$  states and most of our conclusions can be extended straightforwardly to such states.

The zero-field splitting is much larger for  $N=1$  than for  $N=0$  because of the presence of nuclear quadrupole coupling. At low magnetic fields and zero electric field, the microwave spectra display many lines of significant intensity. This persists until the nuclear Zeeman term dominates the zero-field splitting for  $N=1$ . Some of the structure starts to disappear at relatively low magnetic fields,

of as little as a few Gauss, but some persists to fields of thousands of Gauss in systems with large quadrupole coupling constants where one of the nuclear  $g$ -factors is small, such as in  $^{41}\text{K}^{87}\text{Rb}$ . At relatively low fields, it is possible to find 2-photon paths that allow molecules to be transferred between  $N=0$  hyperfine states via  $N=1$  states. However, in the high-field limit the spectra are single-line-dominated and no such paths exist.

An electric field mixes different rotational states and creates orientation and alignment. The oriented states have possible applications in quantum computing [16]. For oriented molecules, the levels correlating with  $N=0$  and 1 both have substantial nuclear quadrupole structure. Even a very small electric field is sufficient to separate the  $N=1$  states with  $M_N=0$  and  $\pm 1$  enough to prevent significant mixing between them. This simplifies the spectrum to some extent. However, the hyperfine levels for  $N=1$  display close avoided crossings as a function of field, which arise at points where the oriented molecules have zero alignment. Even away from the crossings, there is more than one transition with significant intensity at each electric field, and this may cause complications in designing a quantum computer.

Combined electric and magnetic fields provide a conve-

nient way to restore simplicity in the microwave spectra and eliminate unwanted transitions. The magnetic field resolves the near-degeneracy that exists when it is not present.

The calculations described in the present paper are also likely to be important in other applications of ultracold polar molecules, such as in the creation of novel quantum phases [19, 20] and the development of quantum simulators for condensed-phase problems [18, 22]. The spin structure must be taken into account in a full treatment of collisions involving alkali metal dimers.

### Acknowledgments

The authors are grateful to EPSRC for funding the collaborative project QuDipMol under the ESF EURO-CORES Programme EuroQUAM and to the UK National Centre for Computational Chemistry Software for computer facilities. HR is grateful to the China Scholarship Council for funding her joint PhD student program in Durham.

- 
- [1] L. D. Carr, D. DeMille, R. V. Krems, and J. Ye, *New J. Phys.* **11**, 055049 (2009).
- [2] K.-K. Ni, S. Ospelkaus, M. H. G. de Miranda, A. Pe'er, B. Neyenhuis, J. J. Zirbel, S. Kotochigova, P. S. Julienne, D. S. Jin, and J. Ye, *Science* **322**, 231 (2008).
- [3] J. G. Danzl, M. J. Mark, E. Haller, M. Gustavsson, R. Hart, J. Aldegunde, J. M. Hutson, and H.-C. Nägerl, *to be published* (2009).
- [4] K. Winkler, F. Lang, G. Thalhammer, P. van der Straten, R. Grimm, J. Hecker Denschlag, A. J. Daley, A. Kantian, H. P. Büchler, and P. Zoller, *Phys. Rev. Lett.* **98**, 043201 (2007).
- [5] C. Weber, G. Barontini, J. Catani, G. Thalhammer, M. Inguscio, and F. Minardi, *Phys. Rev. A* **78**, 061601(R) (2008).
- [6] A.-C. Voigt, M. Taglieber, L. Costa, T. Aoki, W. Wieser, T. W. Hänsch, and K. Dieckmann, *Phys. Rev. Lett.* **102**, 020405 (2009).
- [7] K. Pilch, A. D. Lange, A. Prantner, G. Kerner, F. Ferlaino, H.-C. Nägerl, and R. Grimm, *Phys. Rev. A* **79**, 042718 (2009).
- [8] J. M. Sage, S. Sainis, T. Bergeman, and D. DeMille, *Phys. Rev. Lett.* **94**, 203001 (2005).
- [9] E. R. Hudson, N. B. Gilfoy, S. Kotochigova, J. M. Sage, and D. DeMille, *Phys. Rev. Lett.* **100**, 203201 (2008).
- [10] M. Viteau, A. Chotia, M. Allegrini, N. Bouloufa, O. Dulieu, D. Comparat, and P. Pillet, *Science* **321**, 232 (2008).
- [11] J. Deiglmayr, A. Grochola, M. Repp, K. Mörtlbauer, C. Glück, J. Lange, O. Dulieu, R. Wester, and M. Weidemüller, *Phys. Rev. Lett.* **101**, 133004 (2008).
- [12] C. Haimberger, J. Kleinert, P. Zabawa, A. Wakin, and N. P. Bigelow, *New J. Phys.* **11**, 055042 (2009).
- [13] J. Aldegunde, B. A. Rivington, P. S. Żuchowski, and J. M. Hutson, *Phys. Rev. A* **78**, 033434 (2008).
- [14] J. Aldegunde and J. M. Hutson, *Phys. Rev. A* **79**, 013401 (2009).
- [15] S. Ospelkaus, K.-K. Ni, G. Quémener, B. Neyenhuis, D. Wang, M. H. G. de Miranda, J. L. Bohn, J. Ye, and D. S. Jin, *arxiv:physics/0908.3931* (2009).
- [16] D. DeMille, *Phys. Rev. Lett.* **88**, 067901 (2002).
- [17] A. André, D. DeMille, J. M. Doyle, M. D. Lukin, S. E. Maxwell, P. Rabl, R. J. Schoelkopf, and P. Zoller, *Nature Physics* **2**, 636 (2006).
- [18] A. Micheli, G. K. Brennen, and P. Zoller, *Nature Physics* **2**, 341 (2006).
- [19] H. P. Büchler, E. Demler, M. Lukin, A. Micheli, N. Prokof'ev, G. Pupillo, and P. Zoller, *Phys. Rev. Lett.* **98**, 060404 (2007).
- [20] A. Micheli, G. Pupillo, H. P. Büchler, and P. Zoller, *Phys. Rev. A* **76**, 043604 (2007).
- [21] A. V. Gorshkov, P. Rabl, G. Pupillo, A. Micheli, P. Zoller, M. D. Lukin, and H. P. Büchler, *Phys. Rev. Lett.* **101**, 073201 (2008).
- [22] M. L. Wall and L. D. Carr, *New J. Phys.* **11**, 055027 (2009).
- [23] D. DeMille, D. R. Glenn, and J. Petricka, *Eur. Phys. J. D.* **31**, 375 (2004).
- [24] M. Wallquist, P. Rabl, M. D. Lukin, and P. Zoller, *New J. Phys.* **10**, 063005 (2008).
- [25] J. Aldegunde, H. Ran, and J. M. Hutson, *arxiv:physics/0905.4489* (2009).
- [26] R. N. Townes and A. L. Schawlow, *Microwave Spectroscopy* (Dover Publications, New York, 1975).
- [27] J. M. Brown and A. Carrington, *Rotational Spectroscopy of Diatomic Molecules* (Cambridge University Press,

- Cambridge, 2003).
- [28] D. L. Bryce and R. E. Wasylshen, *Acc. Chem. Res.* **36**, 327 (2003).
- [29] A. J. Ross, C. Effantin, P. Crozet, and E. Boursey, *J. Phys. B* **23**, L247 (1990).
- [30] P. Staantum, A. Pashov, H. Knöckel, and E. Tiemann, *Phys. Rev. A* **75**, 042513 (2007).
- [31] J. M. Hutson and P. Soldán, *Int. Rev. Phys. Chem.* **25**, 497 (2006).
- [32] T. Köhler, K. Goral, and P. S. Julienne, *Rev. Mod. Phys.* **78**, 1311 (2006).
- [33] N. J. Stone, *At. Data Nucl. Data Tables* **90**, 75 (2005).
- [34] S. Ospelkaus, A. Pe'er, K.-K. Ni, J. J. Zirbel, B. Neyenhuis, S. Kotochigova, P. S. Julienne, J. Ye, and D. S. Jin, *Nature Physics* **4**, 622 (2008).
- [35] M. Aymar and O. Dulieu, *J. Chem. Phys.* **122**, 204302 (2005).